

INTRA-CLUSTER LIGHT AT THE FRONTIER: ABELL 2744

MIREIA MONTES^{1,2} AND IGNACIO TRUJILLO^{1,2}

¹Instituto de Astrofísica de Canarias,c/ Vía Láctea s/n, E38205 - La Laguna, Tenerife, Spain and

²Departamento de Astrofísica, Universidad de La Laguna, E-38205 La Laguna, Tenerife, Spain

Draft version December 3, 2024

ABSTRACT

The ultra-deep multiwavelength HST Frontier Fields coverage of the Abell Cluster 2744 is used to derive the stellar population properties of its intra-cluster light (ICL). The restframe colors of the ICL of this intermediate redshift ($z = 0.3064$) massive cluster are bluer ($g-r \sim 0.7$; $i-J \sim 0.6$) than those found in the stellar populations of its main galaxy members ($g-r \sim 0.85$; $i-J \sim 0.75$). Based on these colors, we derive the following mean metallicity $Z \sim 0.018 \pm 0.003$ for the ICL. The ICL age is $\sim 3 - 5$ Gyr younger than the average age of the massive galaxies of the cluster. The fraction of stellar mass in the ICL component comprises at least 6% of the total stellar mass of the galaxy cluster. Our data is consistent with a scenario where the bulk of the ICL of Abell 2744 has been formed relatively recently ($z < 1$). The stellar population properties of the ICL suggest that this diffuse component is mainly the result of the disruption of infalling galaxies with similar characteristics in mass ($M_* \sim 3 \times 10^{10} M_\odot$) and metallicity than our own Milky Way.

Subject headings: galaxies: clusters: individual (Abell 2744) — galaxies: evolution — galaxies: photometry — galaxies: halos

1. INTRODUCTION

A substantial fraction of stars in clusters are not gravitationally bound to any particular galaxy. These stars constitute the so-called intra-cluster light. The ICL is smoothly distributed around the central galaxy of the cluster and extends to several hundred kpc away from the cluster center. This diffuse light is thought to form primarily by the tidal stripping of stars from galaxies which interact and merge during the hierarchical accretion history of the cluster (e.g. Gregg & West. 1998; Rudick et al. 2006; Conroy et al. 2007; Contini et al. 2014). Therefore, the characterization of the ICL provides a direct way of determining the assembly mechanisms occurring inside galaxy clusters. In this sense, the ICL is the signature of how violent the assembly of the cluster has been through its cosmic history. For that reason, it is absolutely key determining how and when the ICL formed. However, the identification of this light observationally remains difficult and uncertain. Indeed, the typical surface brightness of the ICL is $\mu_V \gtrsim 26.5$ mag/arcsec² (e.g. Mihos et al. 2005; Zibetti et al. 2005; Rudick et al. 2006) and it is contaminated by foreground and background galaxies. Moreover, it is difficult to dissociate between the ICL and the brightest central galaxy surface brightness profile (e.g. Gonzalez et al. 2005).

Although the properties of the stellar populations of the ICL provide a vital tool to understand its formation, little is known about their characteristics. The ICL is reported to be metal-poor in some studies (e.g. Williams et al. 2007) while other studies show super-solar metallicities (e.g. Krick et al. 2006). Simulations predict that the ICL forms very late ($z < 1$; e.g. Contini et al. 2014) and that the bulk of the ICL is produced by the most massive "satellites" ($M_* \sim 10^{10-11} M_\odot$) as they fall into the cluster core. If this scenario

is correct, the ages and metallicities of the intracluster population will be highly dependent on the progenitor galaxies from which they were stripped. Therefore, the ICL is expected to have a metallicity that is similar to that of these massive galaxies. The goal of this paper is to explore this question in detail and characterize, for the first time, the age and metallicity of the ICL of a massive cluster at radial distances $R > 50$ kpc with unprecedented accuracy.

We will achieve our goal taking advantage of the deepest images ever taken by the Hubble Space Telescope (*HST*) of the Abell cluster 2744. The Hubble Frontier Fields¹ (HFF) project represents the largest investment of HST time for deep observations of galaxy clusters. Abell 2744 is the first cluster observed as part of the HFF program. This structure, at $z = 0.3064$ (Owers et al. 2011), is a rich cluster (virial mass of $\sim 7 \times 10^{15} M_\odot$ within $R < 3.7$ Mpc) undergoing a major merger as evidenced by its complex internal structure (Boschin et al. 2006). Therefore, this cluster represents an excellent target for studying the formation of the ICL. The ages and metallicities of the ICL will be studied in detail taking the advantage of the inclusion of the near-infrared (NIR) to break the age-metallicity degeneracy (e.g. Anders et al. 2004).

Throughout this work, we adopt a standard cosmological model with the following parameters: $H_0 = 70$ km s⁻¹ Mpc⁻¹, $\Omega_m = 0.3$ and $\Omega_\Lambda = 0.7$. At $z = 0.3064$, this corresponds to a spatial scale of 4.52 kpc/arcsec.

2. DATA

The data used in this work is based on the first release of the HFF program and includes all the NIR WFC3 data (ID13495, PI: J. Lotz and ID13386, PI: S. Rodney) of Abell 2744. The ACS images were taken from the HST archive as part of the program: ID11689 (PI: R. Dupke)

and consist of six orbits in F435W and five orbits each in F606W and F814W. NIR observations include imaging in four filters F105W, F125W, F140W, F160W based on 24, 12, 10, and 24 orbits, respectively. The data were directly retrieved from the archive². The pixel scale of the drizzled images is $0''.06$. The ($0.4''$ diameter aperture) depth at 5σ of each image is: 27.4 (F435W), 28.0 (F606W), 27.1 (F814W), 28.6 (F105W), 28.5 (F125W), 28.7 (F140W) and 28.2 (F160W) mag (Laporte et al. 2014). The age and metallicity of the ICL is determined using the color information provided by both cameras: ACS and WFC3. Consequently, we will limit our study of the ICL to the common field of view ($\sim 2.0 \times 2.2$ arcmin²).

2.1. Analysis

Our goal is to study the properties of the stellar populations of Abell 2744 down to the faintest surface brightness possible. For this reason, it is necessary to measure accurately the colors of the stellar populations across the cluster. Given that the ACS images are shallower than the WFC3 data, we have spatially re-binned the images of the HFF to improve the S/N and to maximize the detection of the diffuse light of the cluster. Previous to the rebinning, we have smoothed the images with a 5 pixel median box filter to reduce noise, specially in the outer regions of the cluster. The new rebinned pixel value is the sum of 25 input pixels in the original image and has a size of $0.3''$ (~ 1.4 kpc at $z=0.3064$).

Although the HFF data were already processed, our science goal requires exquisite photometry as we are interested in the low surface brightness light. Therefore, we recalculated the background in a clear region, away from the cluster, of the rebinned images and then subtracted it from the whole image.

For the analysis of the ICL, it is crucial to identify the galaxies that are members of the cluster and get rid of background and foreground sources. For this purpose, we build a redshift mask of the cluster image. The mask was constructed using the spectroscopic redshift catalog of Owers et al. (2011) and adding all the photometric redshifts available in NED³. To assign a redshift value to the pixels of the images, first we run SEXTRACTOR in the F160W image to identify the area that correspond to each object. Then, we masked the area subtended by those objects whose redshift do not correspond to the cluster ($z > 0.33$ and $z < 0.27$) and also those without measured redshift. The outer parts of the cluster ($R \gtrsim 180$ kpc) were also masked due to the limitations of the ACS imaging depth to reduce possible contamination due to noise.

2.2. Optical and NIR colors

In order to study the stellar populations of the cluster, including its ICL, we constructed two restframe colors at the redshift of the cluster: $g-r$ and $i-J$. The choice of these colors was made for two reasons: first, to diminish the effects of the different PSFs combining images from the same camera (ACS data for $g-r$ and WFC3 data for $i-J$) and second, to include a NIR filter to constrain the metallicity with better accuracy (e.g. Anders et al.

2004). The colors were built interpolating among the observed filters to obtain the flux in the equivalent rest-frame bands: g , r , i and J .

To explore the stellar populations of Abell 2744 and their variation across the cluster structure, we make use of three independent analysis based on different parameters: the restframe (corrected of cosmological dimming) surface brightness in J -band, μ_J , the logarithm of the stellar mass density, $\log(\rho)$, and the radial distance, R , to the main galaxies of the cluster. These three parameters will allow us to compare our results with theoretical expectations.

The μ_J map of the cluster was divided in seven magnitude bins, from 16 to 24 mag/arcsec². The $\log(\rho)$, an estimation of the mass of the stellar populations, was calculated from the $g-r$ restframe color following equation 1 in Bakos et al. (2008) and the mass to light ratio given in Bell et al. (2003) assuming a Salpeter IMF (Salpeter 1955). The $\log(\rho)$ map of the cluster was divided also in seven mass density bins, from $10^{4.8}$ to $10^{1.6} M_{\odot}/\text{pc}^2$. Finally, we constructed a *radial distance* indicator using the centers of the most massive galaxies in the cluster ($\mu_J < 17$ mag/arcsec²) as the starting points. Then, the distance to their centers was calculated as the elliptical distance defined by the morphological parameters of the galaxies, derived by SEXTRACTOR. The small galaxies of the cluster were masked to reduce the contamination of their different stellar populations at a given radius. This distance was logarithmic spaced in seven bins, from 0 to 85 kpc. We illustrate the different bins separations in Figure 1.

The reason to choose the above parameters, and their binning, is to characterize the stellar populations of the cluster properly, i.e. averaging zones with similar properties. This allows us to describe the cluster from its inner parts (brighter magnitudes, higher densities) to its outer parts (fainter magnitudes, lower densities) in a consistent way. On doing this, the comparison of the ICL properties with those from the cluster galaxies is direct and homogeneous. Consequently, we will infer the properties of the ICL and cluster galaxies based on their relative differences.

In Figure 1, the three color-color diagrams based on the μ_J , $\log(\rho)$ and R maps of the cluster are shown (left panels). A grid of Bruzual & Charlot (2003) models based on a Salpeter IMF for single stellar populations are also plotted. The grid is flagged with their corresponding ages and metallicities. For illustration, in the right panels, the color-coded bins of the three parameters are drawn over an image of the cluster in the F160W band.

3. RESULTS

3.1. Color-color diagrams

The left panels of Figure 1 show the color-color diagrams for each parameter used to characterize the cluster light, i.e. μ_J , $\log(\rho)$ and R . Each data point on the color-color diagram corresponds to the average $g-r$ and $i-J$ color values of the spatial regions drawn in the cluster maps plotted in the right panels. The errors in the $g-r$ and $i-J$ colors are derived from bootstrapping simulations. These simulations consist of 3000 realizations randomly choosing half of the pixels in each bin and calculating their mean colors. The errors represent

² <http://www.stsci.edu/hst/campaigns/frontier-fields/FF-Data>

³ <http://ned.ipac.caltech.edu/>

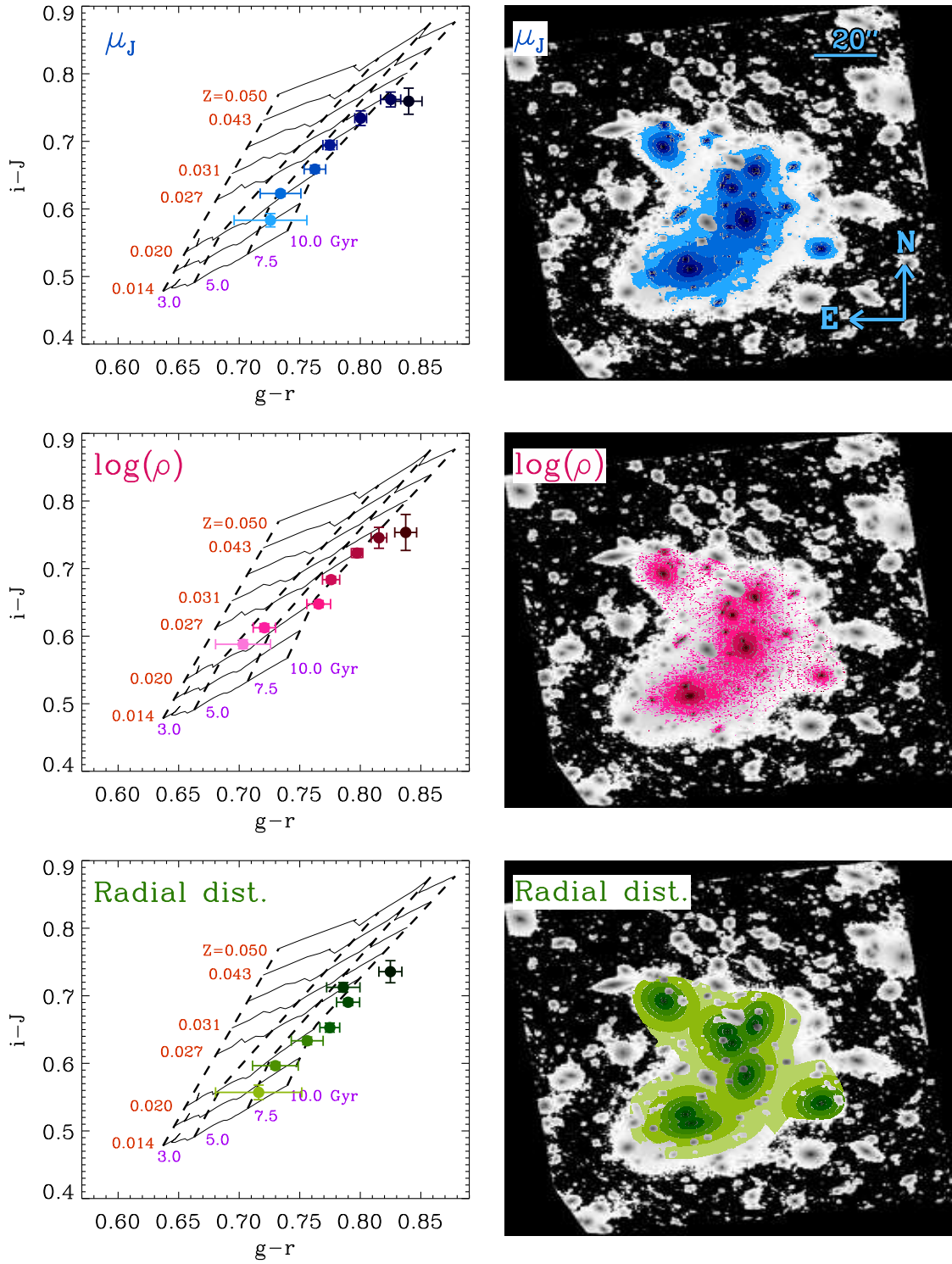


FIG. 1.— Left panels show the $i-J$ vs. $g-r$ diagrams for three different parameters: μ_J (blue), $\log(\rho)$ (pink) and R (green) used to characterize the different spatial regions where the light of the cluster is distributed. Right panels show the image of the cluster in the F160W filter and over-plotted are the different spatial regions in which the colors are measured. The spatial regions are coded from the inner parts of the cluster (darker color) to the outer parts (lighter color).

the scatter of the distributions of the means. These errors account for both the intrinsic scatter of the cluster’s stellar populations and the photometric errors.

For all the color-color diagrams, a continuous blueing of both $g - r$ and $i - J$ colors is clearly seen. Therefore, the stellar populations of the cluster become gradually bluer when moving away from the centers of the galaxies (i.e., towards fainter luminosities and lower densities). According to the values of age and metallicity indicated by the grid of models, this gradient in colors is compatible with a gradient in metallicity, from a supersolar metallicity to a little subsolar, and also a slight gradient in age (see next subsection).

In order to estimate a possible contamination of the colors in the outer regions of the cluster due to the scattered light produced by the different band PSFs, we run the following test. The PSFs for each of the observational bands were modeled using the HST PSF modeling software TINYTIM. Then, we convolved each one of the PSFs with a de Vaucouleurs $r^{1/4}$ profile (de Vaucouleurs 1948) with an effective radius similar to the ones observed in the main galaxies of the cluster. With these convolved profiles, we create the $g - r$ and $i - J$ color profiles. We find that the effect of the different PSFs in the constructed radial colors is less than 1%, suggesting that the measured color gradients are a real property of the cluster’s stellar populations.

3.2. Age and metallicity gradients

To quantify the changes of the stellar populations across the galaxy cluster, we have computed the age and metallicity of the stellar populations based on their $g - r$ and $i - J$ colors. Within each spatial bin, we measure the age and the metallicity of each pixel corresponding to their $g - r$ and $i - J$ colors. Then, we estimate the corresponding mean age and metallicity. As it was done for the colors in the previous section, the errors of the age and metallicity were also drawn from bootstrapping simulations. The gradients of age (upper panels) and metallicity (bottom panels) for each of the parameters are shown in Figure 2. The colors, ages and metallicities for the three parameters are listed in Table A.

In Figure 2, we marked in orange the region tentatively corresponding to the ICL component. Observationally, the exact definition of which part of the cluster light describes the ICL is ill-defined. There have been many different attempts to label the ICL region using criteria as the surface brightness or the radial distance. For instance, Conroy et al. (2007) defined the ICL as the light with $\mu_i > 23.0 \text{ mag/arcsec}^2$ whereas Toledo et al. (2011) used $R > 50 \text{ kpc}$. Depending on the parameter used, we have conservatively defined the ICL region as the region with either $\mu_J > 22.5 \text{ mag/arcsec}^2$, $\log(\rho) < 1.8$ or $R > 50 \text{ kpc}$. The $\log(\rho)$ limit is calculated using the μ_J limit and the color $i - J = 0.6$ (see Fig. 1). These values are inserted into equation 1 in Bakos et al. (2008) with the mass to light ratio in the J -band given by Vazdekis et al. (2012) models for the corresponding age ($\sim 9 \text{ Gyr}$) and metallicity ($Z \sim 0.018$) of the ICL region.

The metallicity within the cluster is continuously decreasing from supersolar ($Z \approx 0.027$) in the central part of the main galaxies to slightly subsolar ($Z \approx 0.018$) in the ICL region. The ICL metallicity is similar to

that found in the stellar halo of nearby massive galaxies (Cocato et al. 2010; Roediger et al. 2011; Greene et al. 2012; Montes et al. 2014). The stellar population ages show a slight negative gradient towards the outskirts. This gradient is compatible with what is found for the giant elliptical galaxy M87 (Liu et al. 2005; Montes et al. 2014), the elliptical galaxies in Roediger et al. (2011) and for some galaxies in Greene et al. (2012).

4. DISCUSSION

State-of-the-art semianalytical models of galaxy formation (i.e. Contini et al. 2014) suggest that the origin of the ICL is the result of disruption and tidal stripping of massive ($10^{10-11} M_\odot$) galaxies infalling in the cluster potential (see also Purcell et al. 2007; Martel et al. 2012). The largest contribution of massive galaxies to the ICL is understood due to the stronger effect of dynamical friction on massive objects compared to the less massive galaxies orbiting the cluster. If the theoretical scenario is correct, we would expect that the mean metallicity of the ICL would be slightly subsolar $Z \sim 0.009 - 0.014$ (corresponding to the typical metallicities of the galaxies described above). Here we find that the mean metallicity of the ICL is slightly subsolar ($Z \sim 0.018 \pm 0.003$), in nice agreement with the theoretical predictions. Using the mass-metallicity relation (Gallazzi et al. 2005), our ICL metallicity corresponds to the metallicities of galaxies with $M_\star \sim 3 \times 10^{10} M_\odot$. This mass and metallicity are similar to that of the Milky Way ($6.43 \pm 0.63 \times 10^{10} M_\odot$, McMillan 2014; $Z \approx 0.02 Z_\odot$, Rix & Bovy 2013). Therefore, the ICL of Abell 2744 can be understood as mainly produced by the disruption of galaxies with similar stellar properties as the Milky Way.

Many theoretical works (e.g. Willman et al. 2004; Monaco et al. 2006; Murante et al. 2007) find that the majority of the ICL formed at $z < 1$. In fact, according to Contini et al. (2014), it is only since $z = 0.4 - 0.5$ that 50% of the ICL of present-day clusters is in place. We find that the ICL age is slightly younger ($\sim 3 - 5 \text{ Gyr}$) than the age of the most massive galaxies of the cluster. This is consistent with the idea that the galaxies that mostly contributed to the ICL were forming stars during a larger period of time than the main galaxies of the cluster. Once the stellar populations were stripped from their progenitor galaxies and start to contribute to the ICL, the star formation of these populations ceased. Consequently, observationally, the data is consistent with a scenario where the ICL formed later than the stars located in the most massive galaxies of the cluster. However, it is not straightforward to say exactly when the ICL in Abell 2744 was produced. Nonetheless, we can speculate on the basis of the difference between the age of the central galaxies and the one found in the ICL⁴. If we assume that the stellar populations of the main galaxies of the cluster were formed at $z \sim 2$ (i.e. $\sim 10 \text{ Gyr}$ ago), then the ICL is compatible with being assembled at $z < 1$.

We can also compare the color of the ICL of Abell 2744 ($g - r \sim 0.7$) with the ICL colors found in other clusters. This color is in agreement with the colors derived for

⁴ We do not use the absolute value of the ages of the stellar populations as it is well known that these values are more prone to errors than their relative differences (e.g. Vazdekis et al. 2001).

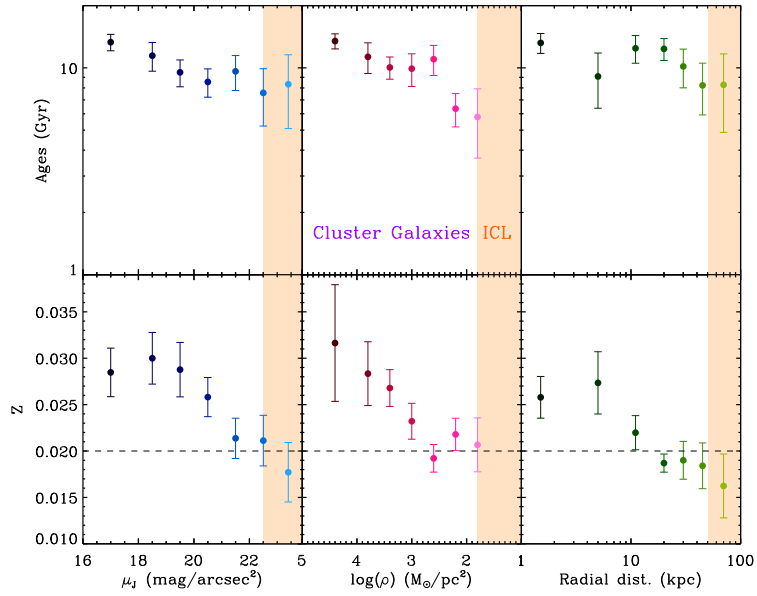


FIG. 2.— Gradients of age and metallicity as a function of μ_J , $\log(\rho)$ and R . The regions corresponding to the cluster galaxies (purple) and the ICL (orange) are labeled. The dashed line marks the solar metallicity.

various tidal features in the Virgo Cluster ($B - V \sim 0.75$, Rudick et al. 2010) and the outskirts of M87 ($g - r \approx 0.72$, Chen et al. 2010, priv. comm.). Covone et al. (2006) also found blue colors for two diffuse features in the cluster Abell 2667 at $z = 0.233$. Our results fit well with the hypothesis that the ICL and the outskirts of the massive galaxies of Abell 2744 may predominantly built-up by the tidal stripping of satellite galaxies.

Finally, another aspect of the ICL that can be directly compared with the theoretical predictions is the fraction of stellar mass of the galaxy cluster that is contained within this component. As we mentioned earlier, the precise definition of what is exactly ICL is observationally ill-defined. Here we have used up to three independent parameters to quantify the spatial region corresponding to the ICL: $\mu_J < 22.5$ mag/arcsec², $\log(\rho) < 1.8$ and $R > 50$ kpc. The amount of stellar mass in the spatial regions defined by those constraints were derived as follows. For $\log(\rho)$ the derivation of the mass was straightforward, while for μ_J and the radial distance we used equation 1 in Bakos et al. (2008) and the corresponding mass to light ratio in the J -band for the age and metallicity of the ICL region (see Figure 2). The total mass of the cluster was obtained similarly but using all the spatial region covered by the light of the cluster explored in this work, including the ICL region. The ICL mass fractions we got are: 6.6% for μ_J , 2.3% for $\log(\rho)$ and 6.7% for the radial distance. Note that these fractions are lower limits of the total contribution of the ICL to the total stellar mass as we are not considering the whole cluster and we are also limited by the depth of the opti-

cal bands (particularly for estimating $\log(\rho)$ based on the $g - r$ color). How our numbers compare with the theoretical expectations? Simulations predict that the fraction of mass in the ICL of present-day galaxy clusters should be around 10%-40% (Contini et al. 2014). At the redshift of our cluster, $z = 0.3$, the fraction of stellar mass in the ICL is expected to be around 60% of today's value. Consequently, we assume that the fraction of mass in a cluster as Abell 2744 would be between 6%-24%. Taking into account that our stellar mass estimates are lower limits, our numbers are in good agreement with theoretical expectations. The simulations are also in nice agreement with other stellar mass fractions measured in other clusters (10%-20%, Feldmeier et al. 2004; Covone et al. 2006; Krick et al. 2006, 2007). Over and over, it seems that the theoretical predictions are reproducing well the observations presented in this work and in other previous papers. We think this is an indication that we are starting to understand the general picture of how this subtle component of the galaxy clusters form.

The results presented in this work show the extraordinary power of the Frontier Fields survey to address the origin and evolution of the ICL. Once the survey will be completed, it will be possible to explore the properties of the ICL in another 5 clusters in the redshift range 0.3 – 0.6; a period of time crucial to understand the formation of this elusive component of the galaxy clusters.

This research has been supported by the Spanish Ministerio de Economía y Competitividad (MINECO; grant AYA2010-21322-C03-02).

REFERENCES

- Anders, P., Bissantz, N., Fritze-v. Alvensleben, U. & de Grijs, R. 2004, MNRAS, 347, 196
- Arnaboldi, M. & Gerhard, O. 2010, Highlights of Astronomy, 15, 97
- Bakos, J., Trujillo, I. & Pohlen, M. 2008, ApJ, 683, L103
- Bell, E. F., McIntosh, D. H., Katz, N. & Weinberg, M. D. 2003, ApJS, 149, 289
- Boschin, W., Girardi, M., Spolaor, M. & Barrena, R. 2006, A&A, 449, 461
- Bruzual, G. & Charlot, S. 2003, MNRAS, 344, 1000
- Chen, C.-W., Côté, P. & West, A. A. 2010, ApJS, 191, 1
- Cocato, L., Gerhard, O. & Arnaboldi, M. 2010, MNRAS, L26
- Conroy, C., Wechsler, R. H. & Kravtsov, A. V. 2007, ApJ, 668, 826
- Contini, E., De Lucia, G., Villalobos, Á. & Borgani, S. 2014, MNRAS, 437, 3787
- Covone, G., Adami, C., Durret, F., et al. 2006, A&A, 460, 381
- de Vaucouleurs, G. 1948, Annales d'Astrophysique, 11, 247
- Feldmeier, J. J., Mihos, J. C., Morrison, H. L., et al. 2004 ApJ, 609, 617
- Ferreras, I., Trujillo, I., Mármol-Queraltó, E. 2013, arXiv:1312.5317
- Gallazzi, A., Charlot, S., Brinchmann, et al. 2005, MNRAS, 362, 41
- Gonzalez, A. H., Zabludoff, A. I. & Zaritsky, D., 2005, ApJ, 666, 147
- Gonzalez, A. H., Zaritsky, D. & Zabludoff, A. I., 2007 ApJ, 666, 147
- Gregg, M. D. & West, M. J., 1998, Nature, 396, 549
- Greene, J. E., Murphy, J. D., Comerford, J. M., et al. 2012, ApJ, 750, 32
- Krick, J. E., Bernstein, R. A. & Pimblet, K. A. 2006, AJ, 131, 168
- Krick, J. E. & Bernstein, R. A. 2007, AJ, 134, 466
- Laporte, N., Streblyanska, A., Clement, B., et al. 2014, A&A, 562, L8
- Liu, Y., Zhou, X., Ma, J., et al. 2005, AJ, 129, 2628
- McMillan, P. J. 2014, MNRAS, 414, 2446
- Martel, H., Barai, P. & Brito, W. 2012, 2012, ApJ, 757, 48
- Mihos, J. C., Harding, P., Feldmeier, J. & Morrison, H. 2005, ApJ, 631, L41
- Monaco, P., Murante, G., Borgani, S. & Fontanot, F. 2006, ApJ, 652, L89
- Montes, M., Trujillo, I., Prieto, M. A. & Acosta-Pulido, J. A. 2014, MNRAS, 439, 990
- Murante, G., Giovalli, M., Gerhard, O., et al. 2007, MNRAS, 377, 2
- Oser, L., Naab, T., Ostriker, J. P., et al. 2012, ApJ, 744, 63
- Owers, M. S., Randall, S. W., Nulsen, P. E. J., et al. 2011, ApJ, 728, 27
- Purcell, C. W., Bullock, J. S. & Zentner, A. R. 2007, ApJ, 666, 20
- Rix, H.-W. & Bovy, J. 2013, A&A Rev., 21, 61
- Roediger, J. C., Courteau, S., MacArthur, L. A. & McDonald, M. 2011, MNRAS, 416, 1996
- Rudick, C. S., Mihos, J. C. & McBride, C. 2006, ApJ, 648, 936
- Rudick, C. S., Mihos, J. C., Harding, P., et al. 2010, ApJ, 720, 569
- Salpeter, E. E. 1955, ApJ, 121, 161
- Toledo, I., Melnick, J., Selman, F. et al. 2011, MNRAS, 414, 602
- Vazdekis, A., Salaris, M., Arimoto, N. & Rose, J. A. 2001, ApJ, 549, 274
- Vazdekis, A., Ricciardelli, E., Cenarro, A. J., et al. 2012, MNRAS, 424, 157
- Williams, B. F., Ciardullo, R., Durrell, P. R., et al. 2007, ApJ, 656, 756
- Willman, B., Governato, F., Wadsley, J. & Quinn, T. 2004, MNRAS, 355, 159
- Zibetti, S., White, S. D. M., Schneider, D. P. & Brinkmann, J. 2005, MNRAS, 358, 949

μ_J (mag/arcsec ²)				
Bin	$g - r$	$i - J$	Age (Gyr)	Z
16-18	0.840 ± 0.011	0.759 ± 0.019	13.3 ± 1.2	0.028 ± 0.003
18-19	0.825 ± 0.008	0.762 ± 0.011	11.4 ± 1.8	0.030 ± 0.003
19-20	0.800 ± 0.005	0.734 ± 0.011	9.5 ± 1.4	0.029 ± 0.003
20-21	0.775 ± 0.006	0.695 ± 0.007	8.5 ± 1.3	0.026 ± 0.002
21-22	0.763 ± 0.009	0.659 ± 0.006	9.6 ± 1.8	0.021 ± 0.002
22-23	0.734 ± 0.017	0.623 ± 0.004	7.5 ± 2.3	0.021 ± 0.003
23-24	0.726 ± 0.030	0.583 ± 0.010	8.3 ± 3.2	0.018 ± 0.003
$\log(\rho(M_\odot/pc^2))$				
4.8-4.0	0.838 ± 0.009	0.753 ± 0.027	13.4 ± 1.1	0.032 ± 0.006
4.0-3.6	0.815 ± 0.006	0.746 ± 0.015	11.3 ± 1.9	0.028 ± 0.003
3.6-3.2	0.797 ± 0.005	0.723 ± 0.007	10.0 ± 1.2	0.027 ± 0.002
3.2-2.8	0.776 ± 0.007	0.684 ± 0.005	9.9 ± 1.7	0.023 ± 0.002
2.8-2.4	0.766 ± 0.010	0.647 ± 0.005	11.0 ± 1.8	0.019 ± 0.001
2.4-2.0	0.721 ± 0.009	0.612 ± 0.006	6.3 ± 1.1	0.022 ± 0.002
2.0-1.6	0.703 ± 0.023	0.588 ± 0.007	5.7 ± 2.1	0.021 ± 0.003
Radial distance (kpc)				
0- 3	0.825 ± 0.009	0.736 ± 0.016	13.2 ± 1.4	0.026 ± 0.002
3- 7	0.786 ± 0.014	0.713 ± 0.007	9.0 ± 2.7	0.027 ± 0.003
7-15	0.790 ± 0.010	0.690 ± 0.005	12.4 ± 1.9	0.022 ± 0.002
15-25	0.775 ± 0.008	0.653 ± 0.007	12.3 ± 1.5	0.019 ± 0.001
25-35	0.756 ± 0.013	0.633 ± 0.006	10.1 ± 2.1	0.019 ± 0.002
35-55	0.730 ± 0.019	0.597 ± 0.005	8.2 ± 2.3	0.018 ± 0.002
55-85	0.716 ± 0.036	0.557 ± 0.011	8.2 ± 3.4	0.016 ± 0.003

TABLE 1
COLORS, AGES AND METALLICITIES WITH THEIR CORRESPONDING ERRORS OF THE CLUSTER ABELL 2744 AS A FUNCTION OF: μ_J , $\log(\rho)$ AND RADIAL DISTANCE.

APPENDIX
COLORS, AGES AND METALLICITIES FOR ABELL 2744